Turkish Journal of Earth Sciences (Turkish J. Earth Sci.), Vol. 20, 2011, pp. 307–320. Copyright ©TÜBİTAK
doi:10.3906/yer-1001-26 First published online 12 October 2010

Sphalerite Associated with Pyrrhotite-Chalcopyrite Ore Occurring in the Kotana Fe-Skarn Deposit (Giresun, NE Turkey): Exsolution or Replacement

EMİN ÇİFTÇİ

İstanbul Technical University, Faculty of Mines, Department of Geological Engineering,
Maslak, TR–34469 İstanbul, Turkey (E-mail: eciftci@itu.edu.tr) (E-mail: nezihi@ kocaeli.edu.tr)

Received 28 January 2010; revised typescripts receipt 13 July 2010 & 07 October 2010; accepted 12 October 2010

Abstract: The Kotana prospect is located about 30 km south of Giresun (NE Turkey). The ore mineralization is a Fe-skarn occurring within the low-grade pre-Lower Jurassic Pınarlar metamorphics, consisting of marble-phyllite intruded by the Upper Cretaceous–Eocene Aksu biotite monzogranite. The principal primary ore minerals include pyrrhotite and magnetite along with minor pyrite (I) and chalcopyrite, accompanied by trace sphalerite. Sphalerite is closely associated with chalcopyrite and to a lesser extent with hexagonal pyrrhotite. Secondary ore minerals include pyrite (II), marcasite, martite, hematite, goethite, lepidocrocite, and intermediate Fe-oxides-hydroxides. Gangue minerals are mainly calcite and quartz. Oxidation of the primary sulphides resulted in formation of diverse secondary ore textures containing bird's eye, martitic, spheroidal, colloform, rim, and veinlets. Distinct crystal shapes of sphalerite are of particular interest to this investigation due mainly to their proposed formation mechanisms. Three alternative mechanisms for their formation were considered: (i) quasi-exsolved bodies developed by hexagonal pyrrhotite replacement of chalcopyrite, (ii) interstitial formation between coalescing pyrrhotite crystals during crystal growth, and (iii) as genuinely exsolved bodies, and as such conflict with previous experimental results. Although the general absence of solute mineral outside the solvent mineral suggests solid solution at high temperatures (favouring the third mechanism), textures, modal, microprobe and sulfur-isotope data suggest that these are more likely to be pseudoexsolved bodies formed as a result of replacement of chalcopyrite by hexagonal pyrrhotite. The $\delta^{34}S$ values of pyrrhotite and chalcopyrite are between 5.23 and 6.73 per mil (n= 12) and 2.29 and 3.26 per mil (n= 8), respectively, indicating continuous enrichment in heavy sulphur isotopes from prograde stage to retrograde stage within the typical range for skarn-type mineralization. Fluid inclusion analyses of calcite and quartz gangues indicate that the minimum homogenization temperature (Th) averaged 400±20 °C with salinities < 15 wt% NaCl equivalent.

Key Words: Eastern Pontides, exsolution, Fe-skarn, pseudoexsolution, pyrrhotite, replacement, sphalerite

Kotana Fe-Skarn Yatağı (Giresun-KD Türkiye)'nda Bulunan Pirotit-Kalkopirit ile ilişkili Sfalerit: Eksolüsyon(mu) veya Ornatım(mı)

Özet: Kotana sahası Giresun (KD Türkiye)'nin yaklaşık 30 km güneyinde bulunmaktadır. Cevher oluşumu bir Fe-skarn olup, Erken Jura öncesi yaşlı mermer-fillitlerden oluşan ve Geç Kretase–Eocene yaşlı Aksu biyotitli monzogranitinin sokulum yaptığı düşük dereceli Pınarlar metamorfitleri içerisinde bulunmaktadır. Başlıca birincil cevher mineralleri pirotit ve magnetit ile minör pirit (I), kalkopirit ve eser sfaleriti içermektedir. Sfalerit varlığı sıkı bir şekilde kalkopiritle, daha az olarak ta pirotitle birliktelik sunmaktadır. İkincil cevher mineralleri pirit (II), markazit, martit, hematite, götit, lepidokrosit ve ara Fe-oksit-hidroksitlerden oluşmaktadır. Gang mineraller esas olarak kalsit ve daha az olarak kuvarstan ibarettir. Birincil sülfürlerin oksidasyonu, kuşgözü, martitik, sferoyidal, koloform, çerçeve ve damarcık gibi çok çeşitli ikincil cevher dokularının oluşumunu sonuçlamıştır. Sfaleritin özgün kristal şekilleri, bu çalışmada, önerilen oluşum mekanizmaları nedeniyle özel bir önem taşımaktadır. Oluşumları için üç alternatif mekanizma dikkate alınmıştır: (i) hegzagonal pirotitin kalkopiriti ornatması sonucu oluşmuş olan yalancı kusma kütleleri olarak oluşmuşlardır, (ii) kristal büyümesi süresince kaynaşan pirotit kristalleri arasında interstisiyal olarak oluşmuşlardır ve (iii) daha önceki deneysel bulguların aksine bunlar gerçek kusma (eksolüsyon) yapılarıdır. Yüksek sıcaklıklarda solüt mineralin solvent mineral dışında genel yokluğu (üçüncü mekanizmayı favori kılmaktadır), dokular, modal-mikroprob ve kükürt izotop verileri bunların olasılıkla kalkopiritin hegzagonal pirotit tarafından ornatılmasının bir sonucu olarak oluşan psöydo-kusma kütleleri olduğunu önermektedir. Pirotit ve kalkopirite ait $\delta^{34}S$ değerleri sırasıyla 5.23 ve 6.73 per mil (n= 12) ve 2.29 ve 3.26 per mil (n= 8) arasında değişmekte bu da, skarn yataklar için tipik aralıkta olmak üzere, prograt safhadan

retrograt safhaya doğru ağır kükürt izotopunca sürekli bir artışı göstermektedir. Kalsit ve kuvars gangları üzerinde yapılan sıvı kapanım analizleri, sülfür cevherleşmesinin ana safhasında minimum oluşum sıcaklığının ortalama 400±20 °C olduğunu ve tuzluluğun < ağ. % 15 NaCl eşdeğer olduğunu göstermektedir.

Anahtar Sözcükler: Doğu Pontitler, eksolüsyon, Fe-skarn, psöydo-eksolüsyon, pirotit, ornatım, sfalerit

Introduction

Many ore minerals undergo exsolution as they cool from the temperatures of initial crystallization. Common examples of exsolution textures that may occur in diverse deposits are blebs (e.g., chalcopyrite in sphalerite), lamellae (e.g., ilmenite in magnetite), flame-like (e.g., pentlandite in pyrrhotite), and myrmekites (e.g., association of arsenic-antimony-stibarsen). Exsolution textures involving natural pyrrhotite as host or guest are listed in Table 1.

The Fe-Zn-S system has the potential for use as a geothermometer and geobarometer to resolve many problems about genesis of an ore deposit provided that the mineral phases formed under required conditions. Many experimental studies deal with phase relations of this system over a large range of temperatures and applications of geothermometer and geobarometer criteria with variable success (Vaughan & Craig 1997 and references therein).

A controversial micro-ore texture, observed between pyrrhotite-sphalerite-chalcopyrite in the Kotana Fe-skarn deposit, in the Dereli area (Giresun, NE Turkey; Figure 1) was studied. Initially the ore textures observed at Kotana were interpreted as conflicting with the conclusions of experimental studies (Barton & Toulmin 1966; Barton & Skinner 1979). However, a single polished section showed a critical transformation between pyrrhotite and chalcopyrite and is the focus of this paper. Three probable mechanisms were discussed, based on the available data. It is found that the replacement mechanism produced an exsolution-like microtexture, and hence such textures occurring elsewhere should be interpreted cautiously.

Geological Framework

The geological structure of the Eastern Pontides (NE Turkey) is the consequence of long-lived subduction, accretion and collision events associated with the closure of the Tethyan Ocean (Okay & Şahintürk 1997 and references therein).

Table 1. Exsolution textures shown by pyrrhotite either as host or guest mineral.

Host	*Guest*	*Nature of Exsolution Pattern*
pyrrhotite	pentlandite	lamellae/flame, myrmekitic
pyrrhotite	chalcopyrite	lamellae/flame
pyrrhotite	magnetite	platelets
pyrrhotite	valleriite	platelets
alabandite	pyrrhotite	blebs
hexagonal pyrrhotite	monoclinic pyrrhotite	curved lamellae/lenses
chalcopyrite	pyrrhotite	stars/crosses
pentlandite	pyrrhotite	emulsion
argentopyrite	pyrrhotite	uniform network
sphalerite	pyrrhotite	blebs in rows
*pyrrhotite	sphalerite	star/stellar/crosses/irregular

*Reported in this study and also by Marignac (1989)

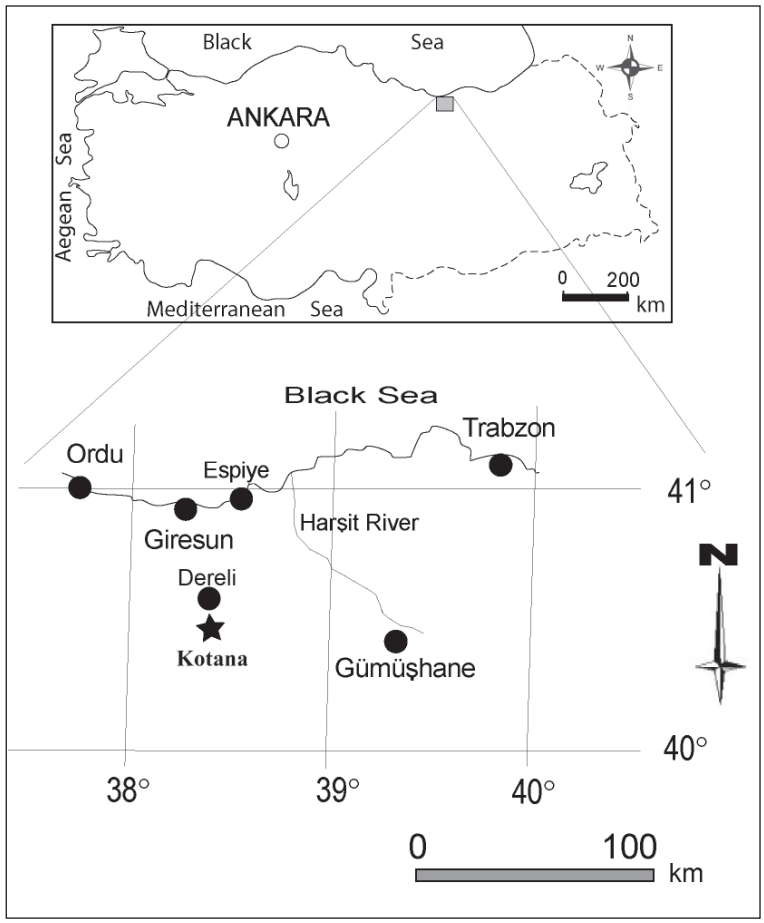

Figure 1. Location map of the study area.

The Eastern Pontides rest generally on pre-Liassic composite basement rocks consisting of (i) high-temperature low-pressure metamorphic units intruded by Lower Carboniferous high-K I-type granitoids (Okay 1996; Topuz & Altherr 2004; Topuz *et al*. 2004a, 2007, 2010), (ii) Permo–Triassic low temperature high pressure metamorphic units (e.g., Okay & Göncüoğlu 2004; Topuz *et al*. 2004b), and (iii) molassic sedimentary rocks of Permo–Carboniferous age (Okay & Leven 1996; Çapkınoğlu 2003). The basement is overlain transgressively by Liassic volcanics and volcaniclastics, deposited in an extensional arc environment. The volcanic members of this sequence are represented by calc-alkaline to tholeiitic basaltic to andesitic rocks (e.g., Şen 2007; Kandemir & Yılmaz 2009). The Liassic volcanics and volcaniclastics grade into Malm–lower Cretaceous carbonates (Okay & Şahintürk 1997 and references therein). Late Cretaceous time is represented by a volcano-sedimentary rock succession more than 2 km thick in the north and by flyschoid sedimentary rocks with limestone olistoliths in the south. Late Cretaceous volcanics compositionally range from basalt to rhyolite (e.g., Eğin & Hirst 1979; Manetti *et al.* 1983; Çamur *et al.* 1996; Arslan *et al.* 1997; Okay & Şahintürk 1997; Boztuğ & Harlavan 2008). Kuroko-type volcanogenic massive sulphide (VMS) deposits are widely associated with Late Cretaceous felsic volcanics (Çiftçi *et al.* 2005 and references therein). The Late Cretaceous magmatism occurred as a result of northward subduction of the İzmir-Ankara-Erzincan Neotethys ocean (e.g., Şengör & Yılmaz 1981; Okay & Şahintürk 1997; Yılmaz *et al.* 1997). The collision between the Eastern Pontides and the Tauride-Anatolide block to the south is constrained to have occurred in the Paleocene to early Eocene

(e.g., Okay & Şahintürk 1997; Okay & Tüysüz 1999). Post-collisional Eocene volcanic and volcaniclastics unconformably overlie the older units, and locally seal the İzmir-Ankara-Erzincan suture (Altherr *et al.* 2008).

As a result of the long-lived subduction and collisional events, the ages of granitoids in the Eastern Pontides range from Early Carboniferous to Late Eocene (e.g., Boztuğ *et al.* 2004; 2005; Topuz *et al.* 2005, 2010; Arslan & Aslan 2006; Karslı *et al.* 2007; Kaygusuz *et al.* 2008; Kaygusuz & Aydınçakır 2009). These granitoids are mostly shallow intrusions, and have well-developed contact aureoles, which have, however, often been neglected (Taner 1977; Sadıklar 1993; Topuz 2006). Within the contact aureoles and their vicinities, numerous skarn-type ore mineralizations of various size and element contents have developed (e.g., Kotana, Özdil and Dokumacılar) (Figure 1).

Kotana Skarn Mineralization

The study area is located in the central portion of the northern zone, but very close to the boundary between the northern and southern zones of the Eastern Pontides, according to the classical division in terms of rock associations (Figure 1). Basement rocks in the area consist of pre-Jurassic Pınarlar metamorphics and overlying post-Jurassic volcaniclastics intruded by the upper Cretaceous–Eocene Aksu monzogranite (78.3±1.5 Ma (Moore *et al.* 1980; Yılmaz & Boztuğ 1996; Saraç 2003). As a consequence, contact metasomatic assemblages were developed locally within the marbles. The Kotana deposit occurs within the marbles of the metamorphic basement, which are generally white, but green in skarns. Hornfelsic rocks are generally green and contain abundant clinopyroxene, garnet and calcite visible to the naked eye. The Kotana skarn is a calcic exso-skarn. Although it does not cover a large area and occurs as discontinuous masses between the ore zone and marble, three distinct zones based on the mineral assemblages were distinguished (Figure 3a): (i) garnet-clinopyroxene, (ii) epidote-garnet-clinopyroxene-calcite, and (iii) epidote; although garnet, clinopyroxene, calcite, scapolite, amphiboles (ferroactinolite, magnesian hornblende, ferrohornblende) micas, quartz, and albite occur in all three zones in varying quantities. Occasional pyritization was also observed.

Although the exact size of the ore body has not been determined, its height and thickness appear to be constant at about 30 m and 15 m, respectively (Figure 3a). The length of the ore body is not known because of faulting, but is estimated at about 0.6 kilometres based on field observations and a number of geological sections. The ore mineralization appears to be a concordant layer with an arcuate shape (Figure

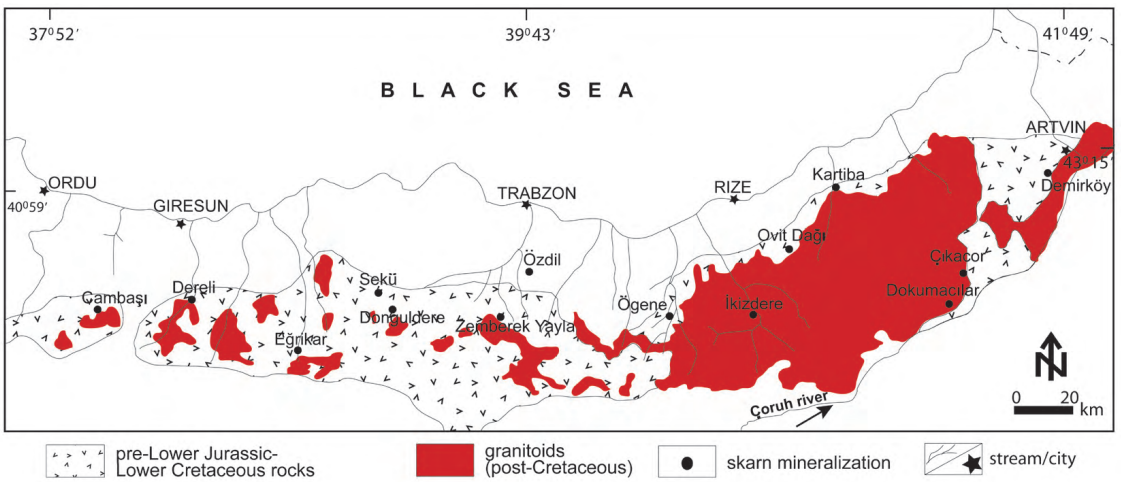

Figure 2. Major contact metasomatic occurrences and associated lithological units along the Eastern Pontide tectonic belt (updated and modified from Aslaner *et al.* 1995).

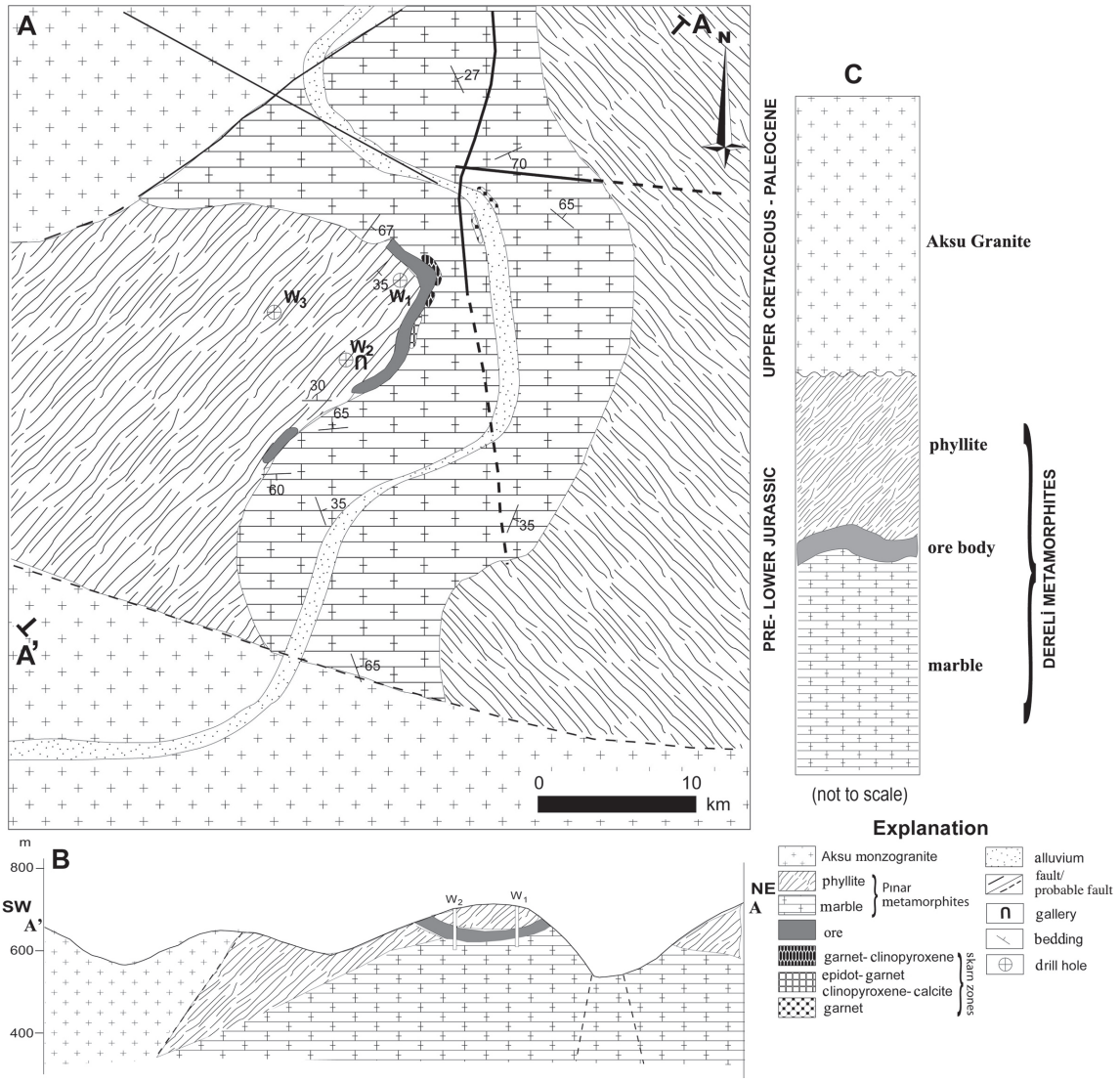

Figure 3. Simplified geological map of the study area **(a)** along with a SW–NE through section **(b)** and a columnar section **(c)** (modified from Van 1977 and Çiftçi & Vıcıl 2003) (size of the ore deposit in all three figures exaggerated).

3b, c). The ore exhibits a somewhat gradual transition from the footwall rocks, but it is cut off sharply at the contact with the hanging-wall rocks. It laterally terminates gradually in one direction and sharply by a fault in the other direction. Proven reserves are about half a million tons with a possible reserve of 1 million tons (Van 1977).

Analytical Methods

Samples examined, considered to be representative for the major ore types of the deposit, were collected from an exploration trench. Polished sections were prepared for both reflected-light microscopy and Electron Probe Microanalysis (EPMA). To obtain the bulk chemical compositions, modal analyses and electron microprobe analyses were carried out using polished sections. Modal analyses were carried out on pyrrhotite and chalcopyrite, both containing sphalerite skeletal inclusions. Digital images were evaluated using SCION image processing software. Pyrrhotite, sphalerite, and chalcopyrite crystals were analyzed for selected elements through point and line analyses by wavelength dispersive X-ray analysis

using a CAMECA SX50 electron microprobe. An accelerating voltage of 15 kV was used. The beam current and counting time for major elements were 20 nA and 20 seconds, respectively. Trace elements were analyzed at a beam current of 100 nA and a counting time of 30 seconds. The accuracy of the EPMA analyses was monitored using reference samples of similar composition (sphalerite, chalcopyrite and pyrrhotite).

On the same polished samples, pyrrhotite and chalcopyrite crystals selected for sulphur isotopic analysis were drilled using a 0.75-mm carbide bit. Mineral powders and a small amount of V_2O_5 were loaded into tin capsules and analyzed using Elemental Analyzer-Continuous Flow Isotope Ratio Mass Spectrometry on a Finnigan MAT252 isotope ratio mass spectrometer (Indiana University, Bloomington, Indiana). Analytical precision is better than ±0.05%.

Analytical results are listed in Tables 2 to 3. Sulphur isotopic compositions are reported in standard δ notation relative to Vienna Canyon Diablo Troilite (VCDT). Listed sulphide analyses are from homogenous crystals through point analyses. Line analysis on a pyrrhotite crystal replacing chalcopyrite was carried out at intervals of 50 micrometers.

The microscope used for fluid inclusions study is a Nikon Optiphot, with x10 oculars, x5, x10, and x40 long working distance lenses. The microscope is fully equipped with transmitted white light. Attached to this microscope is a modified USGS heating and freezing stage, designed by Fluid Inc. USA. This allows microthermometry to be performed on inclusions, by passing heated air over the sample; inclusions can be heated to 700 °C. By passing nitrogen gas passed through liquid nitrogen over the sample, inclusions can be cooled down to –190 °C.

In order to determine the zinc content of typical ore, a representative ore sample was also analyzed by Inductively Coupled Plasma (ICP-ES & MS) (Acme Labs/Canada): a 15 g sample was digested in 90 mL 2-2-2 HCl-HNO_3-H_20 at 95˚C for one hour, was diluted to 300 mL, and then analyzed by employing ICP-ES & MS.

Ore Mineralogy and Micro Ore-textures

Major ore minerals observed in this deposit are hexagonal pyrrhotite (based on PXRD pattern) and magnetite. Chalcopyrite and pyrite locally become significant. Sphalerite and covellite occur in trace quantities. The former is associated mainly with chalcopyrite and, to a lesser extent, hexagonal pyrrhotite. The association of sphalerite with chalcopyrite appears to occur through exsolution; although its association with pyrrhotite is probably due to replacement of chalcopyrite containing exsolved sphalerite by pyrrhotite. A second generation of pyrite, typically fine-grained and intimately intergrown with fine-grained marcasite was also observed and is considered to be a product of

Table 2. EPMA results for selected elements in sphalerite, pyrrhotite and chalcopyrite crystal (results in wt%).

Element	Sphalerite		Pyrrhotite		Chalcopyrite	
	w/Po	w/Cp	w/Sl	w/o Sl	w/Sl	w/o Sl
Fe	9.074	8.524	58.727	60.978	29.582	29.856
Cu	0.180	0.842	0.017	0.008	36.048	34.989
S	33.180	33.112	38.739	37.085	34.547	34.178
Zn	58.001	58.293	0.034	0.017	0.134	0.105
As	0.008	0.015	0.033	0.064	0.023	0.018
Ni	0.003	0.006	nd	0.021	nd	0.017
Co	0.011	0.012	nd	0.003	nd	nd
Bi	nd	nd	0.01	0.136	nd	nd
Cd	0.220	0.200	nd	nd	0.002	nd
Mn	0.017	0.008	nd	nd	nd	nd

*nd: not detected

exsolution from sulphur-rich pyrrhotite. In contrast, the first generation of pyrite occurs as euhedral to subhedral crystals. Martite, hematite, lepidocrocite, and goethite are the principal secondary Fe-oxides, occurring with unidentified intermediate Fe-oxide-hydroxide phases. Quartz and calcite are the major gangue minerals. The presence of twelve more mainly Ca-Fe-Mg-silicates were reported by Çiftçi & Vıcıl (2003).

Microscopic examination of ore textures indicated that the primary sulphide phases (Stage-I sulphides in Figure 5) show mainly simple granular and mosaic ore microtextures, whereas secondary ore textures are much more complicated and varied. During rapid cooling hexagonal pyrrhotite converts to monoclinic pyrrhotite as a stage in the formation of fine-grained pyrite-marcasite mixtures. Where supergene alteration is intense, pyrrhotite alters directly to iron-oxides/hydroxides, which occur as rims surrounding, and veins crosscutting pyrrhotite crystals. Since fine-grained pyrite and marcasite spheroids are especially prone to oxidation, alternating pyrite, marcasite, and iron-oxides-hydroxide layers form concentric spheroids or concentrically grown bands. Marginal weathering of monoclinic pyrrhotite to pyrite and marcasite also resulted in the formation of the so-called 'bird's eye' texture (Figure 4e, h). Figure 5 shows the suggested mineral paragenesis for the deposit.

Experimental Results

Mineral and Bulk Chemistry

A representative ore sample was analyzed for bulk chemistry: Fe (46.6%), Cu (0.098%), Zn (0.04%), Mn (0.02%), Ni (0.003%), Co (0.024%). As, Cd, and Sb were also present, (<0.001 wt%). Based on powder X-ray diffraction (PXRD) and ore microscopy study, pyrrhotite, chalcopyrite, pyrite and sphalerite are the only primary sulphide minerals. Sulphide minerals, together with magnetite, which is the second major phase, account for the bulk chemistry.

Sulfur Isotope Composition

$\delta^{34}S$ values listed in Table 3 were acquired from crystals micro-drilled under stereomicroscope. Most skarns have $\delta^{34}S$ values between about –5 to +8 per mil (Taylor 1987). Data for the sulphide minerals chalcopyrite and pyrrhotite from this deposit fall in this range. However, chalcopyrite has more magmatic values, indicating its early precipitation at probable higher temperatures during the prograde stage (Stage I), dominantly from fluids of magmatic origin and/or less from fluids of non-magmatic origin. Pyrrhotite, on the other hand, crystallized during the retrograde stage (stage II) from fluids relatively more enriched in $\delta^{34}S$, after the first stage sulphide mineralization, due most probably to a combination of declining temperature and the mixing of magmatic waters (low $\delta^{34}S$ values) and meteoric waters (high $\delta^{34}S$ values) that contributed heavy sulphur leached out from country rocks.

Fluid Inclusion Observations

Fluid inclusions determined in calcite and quartz gangues are two phase inclusions, containing liquid and gas phases (L+V). The liquid phases account for more that 70 vol% of the inclusions. The inclusions, isolated within the crystals, non-necked, and not related through fractures or fracture planes, are classified as primary inclusions, based on the criteria described by Roedder (1984) and Van den Kerkhof & Hein (2001), and are used for microthermometric measurements. In the studied samples, no inclusions containing varying volumes of liquid and gas (e.g., >%69 liquid +<%31 vapour, or >%69 vapour + <%31 liquid) at room temperatures that could be an indication for boiling were observed. In all the studied inclusions, homogenization was achieved by total absorption of the gas phase into the liquid phase. Homogenization temperatures (Th), measured in the inclusions, ranged between 380 °C and 460 °C, averaging 400 °C (n= 12). This relatively narrow range is assumed to be the minimum temperature range for the ore mineralization, since magnetite, considered to be a product of the retrograde stage, was also present in some of the samples. Hence, this study suggests that the main sulphide mineralization might have occurred at much higher temperatures. Salinities, calculated based on the last ice melting temperature, were relatively low (< 15 wt% NaCl equivalent) and this is also typical for many skarn-type mineralizations, particularly in the retrograde stage (Meinert 1992).

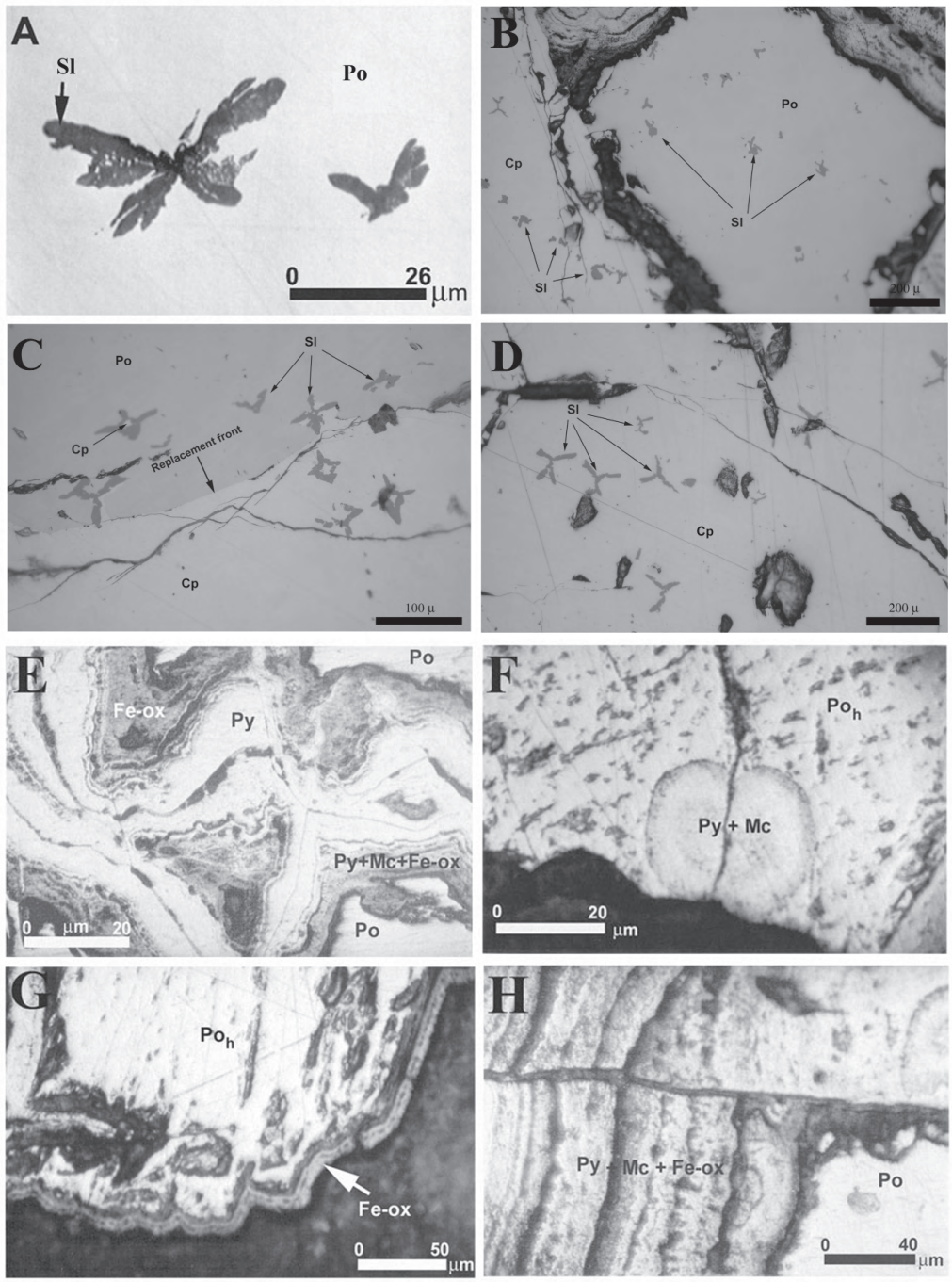

Figure 4. **(A–D)** Butterfly-like exsolved sphalerite bodies in pyrrhotite and chalcopyrite hosts, **(B)** pyrrhotite pseudomorph after chalcopyrite through a complete replacement, **(C)** incomplete replacement of pyrrhotite after chalcopyrite attesting that replacement occurred **(E)** concentric growth bands formed by pyrite and marcasite accompanied by various Fe-oxid es-hydroxides, **(F)** bird's eye texture depeloped by pyrite as a result of pyrrhotite's lateral weathering, **(G)** rim texture resulted from pyrhotite weathering to Fe-oxides, **(H)** close-up view of growth bands containing a repeating succession of pyrite, marcasite, and Fe-oxides (Py– pyrite; Cp– chalcopyrite; Sl– sphalerite; Mc– marcasite; Po– pyrrhotite; Po_h– hexagonal pyrrhotite (Figure 4a is reproduced through scanning and enlarging from Çiftçi & Vıcıl 2003).

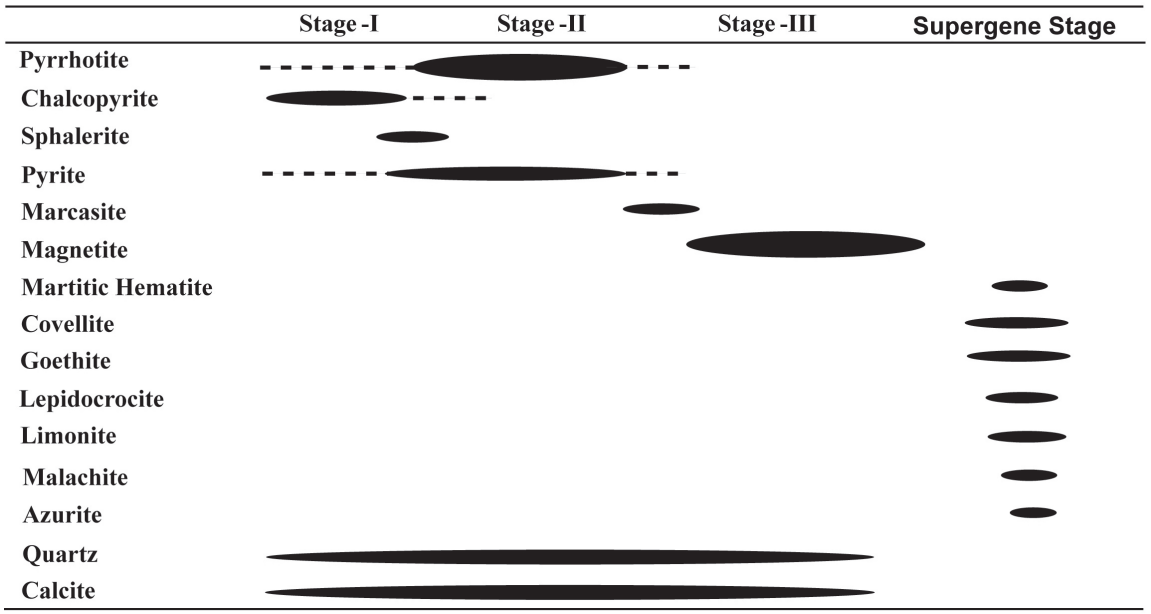

Figure 5. Suggested ore mineral paragenesis for the Kotana deposit: Stage I is considered prograde, Stages II and III are retrograde. In the supergene stage, minerals of the earlier stages are altered to a variety of secondary minerals.

Table 3. Sulfur isotope analysis of pyrrhotite and chalcopyrite crystals (in per mil).

	N	$\delta^{34}S$	Mean	Standard Deviation
Pyrrhotite	12	+5.23 ± 6.73	+ 6.27	±0.48
Chalcopyrite	8	+2.29 ± 3.26	+2.59	±0.36

Discussion

Micrometer-sized grains of sphalerite in chalcopyrite and pyrrhotite hosts form stellate shapes (Figure 4a–c). Micrometer-sized sphalerite exsolution bodies occur as rosettes, star or stellar forms, associated with chalcopyrite as a result of unmixing. Such associations can also come about as a result of a local supersaturation in sphalerite at the growing fronts of chalcopyrite at lower temperatures (e.g., <300 °C), particularly in hydrothermal mineralizations (Marignac 1989). Although distinctions between the two may not be so clear in many cases, in the Kotana mineralization the following observations favour the former explanation for the presence of sphalerite in chalcopyrite (i) sphalerite never occurs as discrete crystals that are not associated with chalcopyrite and pyrrhotite (this is also supported by the bulk analysis of typical ore, since the average zinc content is about 0.04 wt%), (ii) sphalerite is strictly associated with chalcopyrite, (iii) the morphology of sphalerite inclusions are chiefly skeletal, (iv) there is no significant concentration of sphalerite inclusions along chalcopyrite crystal boundaries, (v) the minimum formation temperature for the primary mineral paragenesis is appropriate for the formation of exsolution, considering that skeletal sphalerite begins to dissolve into chalcopyrite at 400 °C (Sugaki & Tashiro 1957), and (vii) the presence of Zn in chalcopyrite within the solubility limits (<0.8 at% or <1.1 wt%) (Sugaki *et al.* 1987) and the presence of skeletal sphalerite within chalcopyrite is always less than about 4 vol% using the bulk analysis. Both the zinc content of the chalcopyrite matrix and observations were based on back-scattered electron images and reflected-light microscope studies: the presence of an intermediate solid solution (ISS) was not considered.

The converse, namely chalcopyrite in sphalerite (chalcopyrite disease) is one of the most common associations in unmetamorphosed epithermal and massive sulphide deposits (Barton & Bethke 1987). In fact, chalcopyrite inclusions in sphalerite are very common and represent, under various circumstances, exsolution and co-precipitation, as well as replacement. There are also reported occurrences of pyrrhotite forming exsolved bodies within sphalerite (Craig & Vaughan 1994; Picot & Johan 1982; Lepetit *et al.* 2003). The reverse association, in the form of sphalerite apparently exsolved from pyrrhotite, is very unusual, although Uytenbogaart & Burke (1985) reported the presence of sphalerite inclusions within pyrrhotite and oriented intergrowths between pyrrhotite and sphalerite, and Ramdohr (1980, p. 602) mentioned the presence of thin plates of a sphalerite-like mineral in pyrrhotite. The underlying reason is that the solubility of zinc sulphide in pyrrhotite is very low. However, despite the observation of Barton & Toulmin (1966) of limited Zn solubility in pyrrhotite and ability of pyrrhotite to dissolve less than 0.1% ZnS (Barton & Skinner 1979; p. 366), the ore microtextures strongly suggest that sphalerite exsolved from pyrrhotite (Figure 4a, b). Thus, this particular texture presents a contradiction.

Ore microscopy indicated that sphalerite occurred only in chalcopyrite and pyrrhotite. In principle, complex sphalerite crystal outlines can be produced through a number of combinations of coalescing pyrrhotite crystals as shown in Figure 6. However, the sphalerite association with pyrrhotite would be expected irrespective of the presence of chalcopyrite, in such a hypothetical scenario. Ore microscopy study ruled out the possibility of this mechanism, because chalcopyrite was always part of the occurrence.

A second and more probable mechanism that could produce such a texture is replacement of the original host chalcopyrite by pyrrhotite. Through replacement, exsolved sphalerite bodies originally within chalcopyrite could be preserved even though the parent mineral, chalcopyrite, was completely replaced. EPMA analyses of pyrrhotite crystals with and without sphalerite masses indicated that the only significant difference is in Cu and Zn contents, which were enriched in pyrrhotite containing sphalerite bodies (Table 2) that were originally chalcopyrite (Figure 4b). Line analyses crossing the chalcopyrite-pyrrhotite interface show a gradual decrease in Cu as the replacement front advanced. The advance left behind the exsolved sphalerite as a record of the process. Some of the fractures in chalcopyrite continue into replacing pyrrhotite, whereas reverse occurrence was not observed, thereby indicating the pseudomorphous replacement of chalcopyrite (Figure 7) resulting in the formation of quasi-exsolved bodies of sphalerite in pyrrhotite. Figures 4c and 7 both show the sphalerite stars straddling the chalcopyrite-pyrrhotite boundary that could be considered as another indication of the process.

A significant portion of dissolved copper would be expected to precipitate as copper rich species requiring less sulphur, although due to decreasing temperature and sulphur fugacity, some of that copper may probably have left the system. However, minor to trace malachite could account for some of the copper produced during the replacement processes. The replacement might have been driven by introduction of Fe^{2+} in a reaction such as

$$CuFeS_2 + Fe^{++} + 0.5\ H_2 = 2\ FeS + Cu^{+} + H^{+}$$

but the real reaction must be more complex to allow for pyrrhotite of $Fe_{(1-x)}S$ composition and also to accommodate volume changes during replacement. Furthermore, declining temperature and sulphur fugacity are scarcely the primary drivers here.

The only significant difference in the mineral chemistry between chalcopyrite with and without sphalerite was in copper content and, to lesser extent, contents of zinc and cadmium. Chalcopyrite without sphalerite was comparatively low in copper since some of the copper ions were substituted by zinc. However, in chalcopyrite with sphalerite, zinc was exsolved as sphalerite, leaving copper sites in chalcopyrite filled only by copper, resulting in chalcopyrite enriched in copper. Zinc and cadmium contents were also higher in chalcopyrite containing sphalerite masses. This is because Cd prefers sphalerite as a host; therefore, as sphalerite exsolves the Cd goes into the sphalerite. Line analyses also showed that points closer to sphalerite bodies are significantly low or nil in zinc content.

However, many convincing data came from the EPMA of sphalerite bodies in both pyrrhotite and

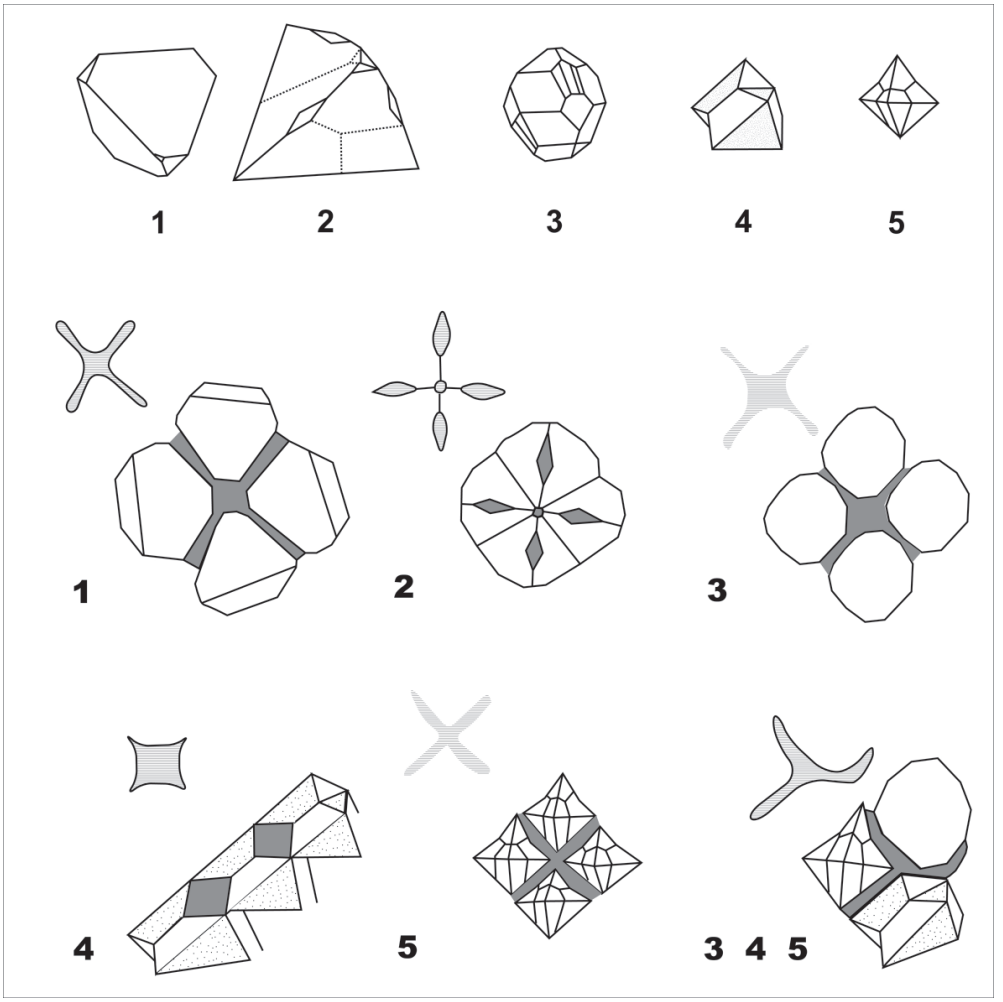

Figure 6. Simplified sketch of coalescing pyrrhotite crystals (1 through 5) that could entrap intergranular sphalerite that would lead to exsolution-like textures (constructed through personal communication with M. Vıcıl).

chalcopyrite. The chemistry was strikingly similar (Table 2, Figure 8) favouring the scenario wherein chalcopyrite crystallized during prograde stage I and exsolved sphalerite under conditions that were more magmatic (as indicated by the sulphur isotope data). Pyrrhotite was subsequently deposited during retrograde stage II under low sulphur fugacity and more dilute conditions with respect to source of sulphur, under conditions that become suitable for massive magnetite deposition later in the retrograde stage. The modal analyses of pyrrhotite containing skeletal sphalerite yielded very similar results (< 4 vol%) to those acquired from the chalcopyrite. This ruled out the possibility of sphalerite being real exsolved bodies in pyrrhotite (the third mechanism). Micro-analytical data with ore microscopy indicated that this particular texture was brought about as a result of pyrrhotite replacement of chalcopyrite that already contained exsolved sphalerite bodies, thus forming the exsolution-like ore texture.

Acknowledgement

This project was funded by the Scientific and Technological Research Council of Turkey (TÜBİTAK; Project Code: 2219). The author thanks Paul B. Barton (USGS), Richard D. Hagni (Missouri University of Science and Technology,

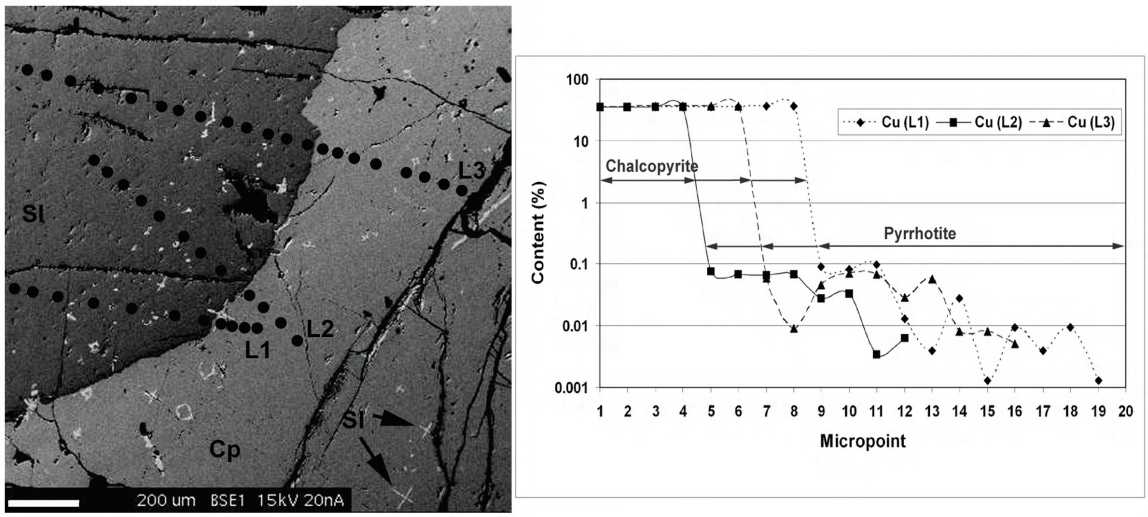

Figure 7. BSE image of incomplete replacement of chalcopyrite by pyrrhotite and microanalysis along selected 3 lines. Dark solid dots indicate micropoints analyzed. Along three lines within the darker phase (pyrrhotite), copper content decreases as the replacement front advances.

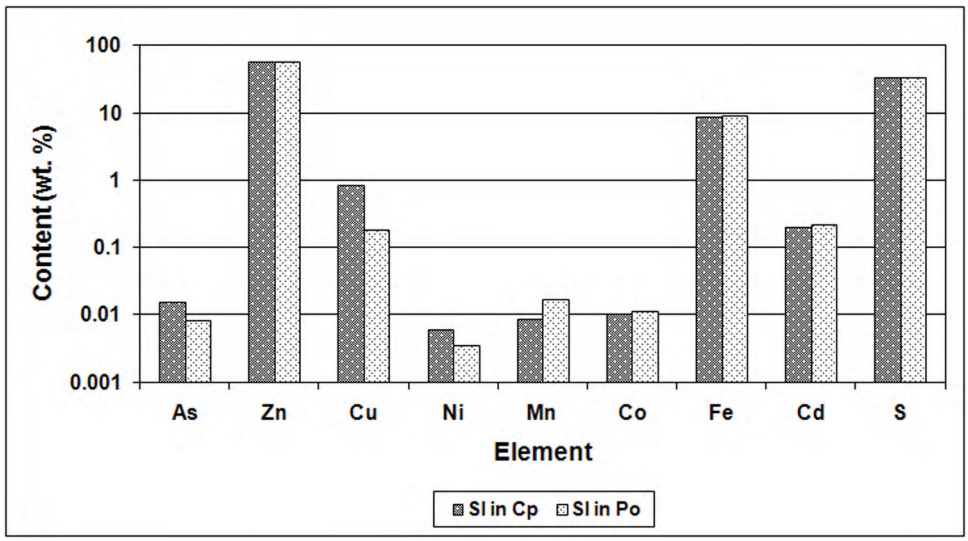

Figure 8. EPMA values of major and common elements of sphalerite hosted both by chalcopyrite and pyrrhotite.

USA), İ. Kuşçu (Muğla University), and Dr. G. Topuz (İstanbul Technical University) for their careful reading of the manuscript and comments on the ore textures and the regional geology, respectively. Their contributions and constructive criticisms significantly improved the manuscript. I am also indebted to Edward M. Ripley and Chusi Li (Indiana University, Bloomington, USA) for their kind help for EPMA and sulphur isotope analysis carried out at their facilities and to N. Hanilçi (İstanbul University) for his help on interpretation of fluid inclusion data and to M. Vıcıl (Karadeniz Technical University) for sample acquisition and for constructing Figure 6.

References

Altherr, R., Topuz, G., Siebel, W., Şen, C., Meyer, H.-P., Satır, M. & Lahaye, Y. 2008. Geochemical and Sr-Nd-Pb isotopic characteristics of Paleocene plagioleucitites from the Eastern Pontides (NE Turkey). *Lithos* **105**, 149–161.

Arslan, M. & Aslan, Z. 2006. Mineralogy, petrography and whole-rock geochemistry of the Tertiary granitic intrusions in the Eastern Pontides, Turkey. *Journal of Asian Earth Sciences* **27**, 177–193.

Arslan, M., Tüysüz, N., Korkmaz, N. & Kurt, H. 1997. Geochemistry and petrogenesis of the Eastern Pontide volcanic rocks, Northeastern Turkey. *Chemie der Erde* **57**, 157–187.

Aslaner, M., Van, A. & Yalçınalp, B. 1995. General features of the Pontide metallogenic belt. *In:* Erler, A., Ercan, T., Bingöl, E. & Örçen, S. (eds), *Geology of the Black Sea Region.* General Directorate of Mineral Research and Exploration and Chamber of Geological Engineers, Ankara, Turkey, 209–213.

Barton, P.B. & Bethke, P.M. 1987. Chalcopyrite disease of sphalerite: pathology and epidemiology. *American Mineralogist* **72**, 451–467.

Barton, P.B. & Skinner, B.J. 1979. Sulfide mineral stabilities. *In:* Barnes, H.L. (ed), *Geochemistry of Hydrothermal Ore Deposits*. 2nd Edition, Wiley& Sons, New York.

Barton, P.B. & Toulmin, P. 1966. Phase relations involving sphalerite in the Fe-Zn-S system. *Econic Geol*ogy **61**, 815–849.

Boztuğ, D., Erçin, A.I., Kuruçelik, M.K., Göç, D., Kömür, İ. & İskenderoğlu, A. 2006. Geochemical characteristics of the composite Kaçkar batholith generated in a Neo-Tethyan convergence system, Eastern Pontides, Turkey. *Journal of Asian Earth Sciences* **27**, 286–302.

Boztuğ, D. & Harlavan, Y. 2008. K-Ar ages of granitoids unravel the stages of Neo-Tethyan convergence in the eastern Pontides and central Anatolia, Turkey. *International Journal of Earth Sciences* **97**, 585–599.

Boztuğ, D., Jonckheere, R., Wagner, G.A. & Yeğingil, Z. 2004. Slow Senonian and fast Palaeocene–Early Eocene uplift of the granitoids in the central eastern Pontides, Turkey: apatite fissiontrack results. *Tectonophysics* **382**, 213–228.

Çamur, M.Z., Güven, İ.H. & Er, M. 1996. Geochemical characteristics of the Eastern Pontide volcanics, Turkey: An example of multiple volcanic cycles in the arc evolution. *Turkish Journal of Earth Sciences* **5**, 123–144.

Çapkinoğlu, Ş. 2003. First records of conodonts from the Permo-Carboniferous of Demirözü (Bayburt), Eastern Pontides, NE Turkey. *Turkish Journal of Earth Sciences* **12**, 199–217.

Çiftçi, E. 2000. *Mineralogy, Paragenetic Sequence, Geochemistry, and Genesis of the Gold and Silver Bearing Upper Cretaceous Mineral Deposits, Northeastern Turkey.* PhD Thesis, University of Missouri-Rolla, Missouri-USA [unpublished]. **NOT CITED IN THE TEXT!..**

Çiftçi, E., Kolayli, H. & Tokel, S. 2005. Lead-arsenic soil geochemical study as an exploration guide over the Killik volcanogenic massive sulfide deposit, Northeastern Turkey. *Journal of Geochemical Exploration* **86**, 49–59.

Çiftçi, E. & Vicil, M. 2003. Kurtulmuş iron Mineralization – an example to the skarn-type ore deposits from Eastern Pontides (Giresun, NE Turkey). *Geosound* **26**, 79–92.

Craig, J.B. & Vaughan, D.J. 1994. *Ore Microscopy and Ore Petrography*. 2nd Edition. Wiley-Interscience, New York.

Eğin, D. & Hirst, D.M. 1979. Tectonic and magmatic evolution of volcanic rocks from the northern Harşit river area, NE Turkey. *Proceedings of Geocome 1 (the 1st Geological Congress on the Middle East)*. Mineral Research and Exploration of Turkey (MTA) Publications, 56–93.

Kandemir, R. & Yilmaz, C. 2009. Lithostratigraphy, facies, and deposition environment of the lower Jurassic Ammonitico Rosso type sediments (ARTS) in the Gümüşhane area, NE Turkey: implications for the opening of the northern branch of the Neo-Tethys Ocean. *Journal of Asian Earth Sciences* **34**, 586–598.

Karsli, O., Chen, B., Aydin, F. & Şen, C. 2007. Geochemical and Sr-Nd-Pb isotopic compositions of the Eocene Dölek and Sariçiçek plutons, Eastern Turkey: implications for magma interaction in the genesis of high-K calc-alkaline granitoids in a post-collision extensional setting. *Lithos* **98**, 67–96.

Kaygusuz, A. & Aydinçakir, E. 2009. Mineralogy, whole-rock and Sr-Nd isotope geochemistry of mafic microgranular enclaves in Cretaceous Dağbaşı granitoids, Eastern Pontides, NE Turkey: evidence of magma mixing, mingling and chemical equilibration. *Chemie der Erde* **69**, 247–277.

Kaygusuz, A., Siebel, W., Şen, C. & Satir, M. 2008. Petrochemistry and petrology of I-type granitoids in an arc setting: the composite Torul pluton, Eastern Pontides, NE Turkey. *International Journal of Earth Sciences* **97**, 739–764.

Lepetit, P., Bente, K., Doering, T. & Luckhaus, S. 2003. Crystal chemistry of Fe-containing sphalerites. *Physics and Chemistry of Minerals* **30**, 185–191.

Manetti, P., Peccerillo, A., Poli, G. & Corsini, F. 1983. Petrochemical constraints on the models of Cretaceous–Eocene tectonic evolution of the Eastern Pontic chain (Turkey). *Cretaceous Research* **4**, 159–172.

Marignac, CH. 1989. Sphalerite stars in chalcopyrite: are they always the result of an unmixing process? *Mineralium Deposita* **24**, 176–182.

Meinert, L.D. 1992. Skarn and skarn deposit. *Geoscience Canada* **19**, 145–162.

Moore, W.J., Mckee, E.H. & Akinci, Ö. 1980. Chemistry and chronology of plutonic rocks in the Pontide Mountains, northern Turkey. *European Copper Deposits,* 209–216, Belgrade.

Okay, A.I. 1996. Granulite facies gneisses from the Pulur region, Eastern Pontides. *Turkish Journal of Earth Sciences* **5**, 55–61.

Okay, A.I. & Göncüoğlu, M.C. 2004. Karakaya Complex: a review of data and concepts. *Turkish Journal of Earth Sciences* **13**, 77–95.

Okay, A.I. & Leven, E.J.A. 1996. Stratigraphy and paleontology of the Upper Paleozoic sequence in the Pulur (Bayburt) region, Eastern Pontides. *Turkish Journal of Earth Sciences* **5**, 145–155.

Okay, A.I. & Şahİntürk, Ö. 1997. Geology of the Eastern Pontides. *In*: Robinson, A.G. (ed), *Regional and Petroleum Geology of the Black Sea and Surrounding Region*. American Association of Petroleum Geologists *(AAPG) Memoir* **68**, 291–311.

Okay, A.I. & Tüysüz, O. 1999. Tethyan sutures of northern Turkey. *In*: Durand, B., Jolivet, L. & Horváth, F., Séranne, M. (eds), The *Mediterranean Basins: Tertiary Extension within the Alpine Orogen*. Geological Society, London, Special Publications **156**, 475–515.

Picot, P. & Johan, Z. 1982. *Atlas of Ore Minerals*. BRGM/Elsevier, Orleans, France/Amsterdam, The Netherlands.

Ramdohr, P. 1980. *The Ore Minerals and their Intergrowths: Volumes 1 & 2*. Pergamon Press, Oxford.

Roedder, E. 1984. *Fluid inclusions. Reviews in Mineralogy, Volume 12*. Book Crafters, Inc, Michigan.

Sadiklar, M.B. 1993. Granat-pyroxene-rhytmite bei Ozdil/Trabzon, NETurkei. *Chemie der Erde* **53**, 341–353.

Saraç, S. 2003. *Doğu Karadeniz Bölgesi Demirli Skarn Yataklarının Karşılaştırılmalı Mineralojik ve Jeokimyasal Özellikleri [Comparative Mineralogic and Geochemical Characteristics of East Black Sea Region Scarn Deposits]*. PhD Thesis, Karadeniz Technical University, 259 p [in Turkish with English abstract, unpublished].

Sugaki, A. & Tashiro, C. 1957. Thermal studies on the skeletal crystals of sphalerite in chalcopyrite. *Science Report, Tohoku University* **3-5**, 293–304.

Sugaki, A., Kitakaze, A. & Kojima, S. 1987. Bulk compositions of intimate intergrowths of chalcopyrite and sphalerite and their genetic implications. *Mineralium Deposita* **22**, 26–32.

Şen, C. 2007. Jurassic volcanism in the Eastern Pontides: is it rift related or subduction related? *Turkish Journal of Earth Sciences* **16**, 523–539.

Şengör, A.M.C. & Yilmaz, Y. 1981. Tethyan evolution of Turkey: a plate tectonic approach. *Tectonophysics* **75**, 181–241.

Taner, M.F. 1977. *Etude géologique et petrographique de la region de Guneyce-Ikizdere, située au sud de Rize (Pontides orientales, Turquie)*. PhD Thesis, University of Geneve, [in French, unpublished].

Taylor, B.E. 1987. Stable isotope geochemistry of ore-forming fluids. *In:* Kyser, K. (ed), *Stable Isotope Geochemistry of Low Temperature Fluids.* Mineralogical Association of Canada Short Course **13**, 337–445.

Topuz, G. 2006. Contact metamorphism around the Eocene Saraycık Granodiorite, eastern Pontides, Turkey. *Turkish Journal of Earth Sciences* **15**, 75–94.

Topuz, G. & Altherr, R. 2004. Pervasive rehydration of granulites during exhumation – an example from the Pulur complex, Eastern Pontides, Turkey. *Mineralogy and Petrology* **81**, 165–185.

Topuz, G., Altherr, R., Kalt, A., Satir, M., Werner, O. & Schwarz, W.H. 2004a. Aluminous granulites from the Pulur complex, NE Turkey: a case of partial melting, efficient melt extraction and crystallization. *Lithos* **72**, 183–207.

Topuz, G., Altherr, R., Kalt, A., Satir, M. & Schwarz, W.H. 2004b. Low-grade metamorphic rocks from the Pulur complex, NE Turkey: implications for pre-Liassic evolution of the Eastern Pontides. *International Journal of Earth Sciences* **93**, 72–91.

Topuz, G., Altherr, R., Schwarz, W.H., Siebel, W., Satir, M. & Dokuz, A. 2005. Post-collisional plutonism with adakite-like signatures: the Eocene Saraycık granodiorite (Eastern Pontides, Turkey). *Contributions to Mineralogy and Petrology* **150**, 441–455.

Topuz, G., Altherr, R., Schwarz, W.H., Dokuz, A. & Meyer, H.-P. 2007. Variscan amphibolite facies metamorphic rocks from the Kurtoğlu metamorphic complex (Gümüşhane area, Eastern Pontides, Turkey). *International Journal of Earth Sciences* **96**, 861–873.

Topuz, G., Altherr, R., Schwarz, W.H., Zack, T., Hasözbek, A., Barth, M., Satir, M. & Şen, C. 2010. Late Carboniferous high-potassium I-type granitoid magmatism in the Eastern Pontides: the Gümüşhane pluton (NE Turkey). *Lithos* **116**, 92–119.

Uytenbogaart, W. & Burke, E.A.J. 1971. *Tables for Microscopic Identification of Ore Minerals.* Elsevier, Amsterdam.

Van, A. 1977. *Giresun-Dereli Kurtulmuş Köyü Fe Zuhuruna Ait 1:10.000 Ölçekli Jeoloji Haritası [1:10.000 Scale Mapping of Giresun-Dereli Kurtulmuş Village Fe-deposit]*. Mineral Research and Exploration Institute of Turkey Report no. **33147** [in Turkish, unpublished].

Van Den Kerkhof, A.M. & Hein, U.F. 2001. Fluid inclusion petrography. *Lithos* **55**, 27–47.

Vaughan, D.J. & Craig, J.B. 1997. Sulfide Ore Mineral Stabilities, Morphologies, and Intergrowth Textures. *In:* Barnes, H.L. (ed), *Geochemistry of Hydrothermal Ore Deposits.* 3rd Edition, Wiley& Sons, New York.

Yilmaz, S. & Boztuğ, D. 1996. Space and time relations of three plutonic phases in the Eastern Pontides, Turkey. *International Geology Review* **38**, 935–956.

Yilmaz, Y., Tüysüz, O., Yiğİtbaş, E., Genç Ş.C. & Şengör, A.M.C. 1997. Geology and tectonic evolution of the Pontides. *In*: Robinson, A.G. (ed), *Regional and Petroleum Geology of the Black Sea and Surrounding Region*. American Association of Petroleum Geologists (AAPG) Memoir **68**, 183–226.